

# BORE-INDUCED MACROVORTICES OVER A PLANAR BEACH: THE CROSS-SEA CONDITION CASE

Matteo Postacchini<sup>1</sup>, Maurizio Brocchini<sup>2</sup> and Luciano Soldini<sup>3</sup>

Wave breaking over submerged topographic obstacles leads to vorticity generation and, at times, to the generation of strong offshore-directed rip currents. The generation of finite-length breakers may also be induced by the positive interaction of wave trains propagating to shore with a relative angle. Such an interaction gives rise to a short-crested system, this, in turn, generating both breakers of finite crossflow length and an intense associated vorticity. We here analyze such a vorticity generation mechanism specifically focusing on the location where wave breaking occurs. To this purpose we both derive a simple theory, based on the well-known theory of wave ray propagation, and perform ad-hoc numerical simulations, using a NSWE (Nonlinear Shallow Water Equations) solver. A fairly good comparison between such preliminary theoretical and numerical results suggests that the present work be used as the basis for future analyses of vorticity generation by cross-seas.

*Keywords: cross sea; ray theory; breaking; Nonlinear Shallow Water Equations*

## INTRODUCTION

Many sandy beaches are characterized by the presence of submerged obstacles, be they either natural (e.g. bars generated by significant sea storms) or manmade (e.g. rubble-mound breakwaters). As a consequence of significant sea storms and obstacles of finite longshore length waves break over and a vortex generates at each of its edges. The complex mechanism, described in Brocchini et al. (2004), evolves leading to the detachment of the vortices from the obstacle edges and to their migration, either to the onshore or to the offshore. Such a migration occurs in response to three different mechanisms that play the main role in the propagation of macrovortices in the nearshore region, especially in the gap between contiguous bars or breakwaters: i) acceleration of the background flow, ii) self-advection by sloping beds and iii) mutual advection by oppositely-signed vortices.

Brocchini et al. (2004) showed how, in the presence of isolated breakwaters, a vortex generates at each edge of the barrier, slowly propagates along the barrier, then detaches and moves towards the shoreline: such a behavior was confirmed by numerical simulations run using a NSWE (Nonlinear Shallow Water Equations) solver, that also illustrate the beach slope influence on the vortex trajectory.

On the other side, Kennedy et al. (2006) analyzed three different cases, by mean of both laboratory experiments and Boussinesq-type numerical simulations, of the vortex generation and migration at nearby breakwaters. For what concerns the vorticity patterns both upstream and downstream of the breakwater, the influence of the gap between contiguous breakwater was investigated, also obtaining a good agreement between experiments and numerical tests. In the case of very wide gaps (isolated-breakwater case), some vortices generate at the breakwater heads, move toward the offshore, following a diagonal path to the shoreline, and their motion is forced only the self-advection due to the beach slope. In the cases of very small gaps between the barriers, the vortices migrate to the offshore and, besides being self advected, they undergo intense mutual advection.

The latter cases highlight a typical behavior that occurs at neighboring breakwaters, i.e. the generation of rip currents, that are more pronounced when the gap is narrow. Hence, the connection between such currents, associated with different water levels between the inshore and the offshore side of the beach, and mutual advection of seaward-directed vortices, is fundamental to understand the hydrodynamics, and, furthermore, the morphodynamics, occurring at a protected beach.

The described vortex generation and evolution are a direct consequence of the finite-length breakers that arise when a wave overpasses a submerged obstacle. Another phenomenon may lead to the generation of breakers of finite crossflow length, i.e. the positive interaction of wave trains traveling from the offshore to the inshore with a different inclination: we call this the “cross-sea condition” (see Fig. 1, top left panel). The interaction between waves approaching the shore from different directions generates a sort of short-crested system (bottom left panel of Fig. 1), as suggested by Silvester (1974). Crests and troughs intersect, this leading to much smaller minimum water levels and much larger

---

<sup>1</sup> DICEA, Università Politecnica delle Marche, Via Brecce Bianche, Ancona, 60131, Italy

<sup>2</sup> DICEA, Università Politecnica delle Marche, Via Brecce Bianche, Ancona, 60131, Italy

<sup>3</sup> DICEA, Università Politecnica delle Marche, Via Brecce Bianche, Ancona, 60131, Italy

maximum water levels, with respect to a single wave train. Hence, breaking occurs earlier, i.e. at larger depths, and the breaker is characterized by a finite length, like in the case of submerged obstacles. The larger wave heights generate both an intense vorticity nearby the breaking location and a strong motion close to the seabed, thus inducing significant sediment transport.

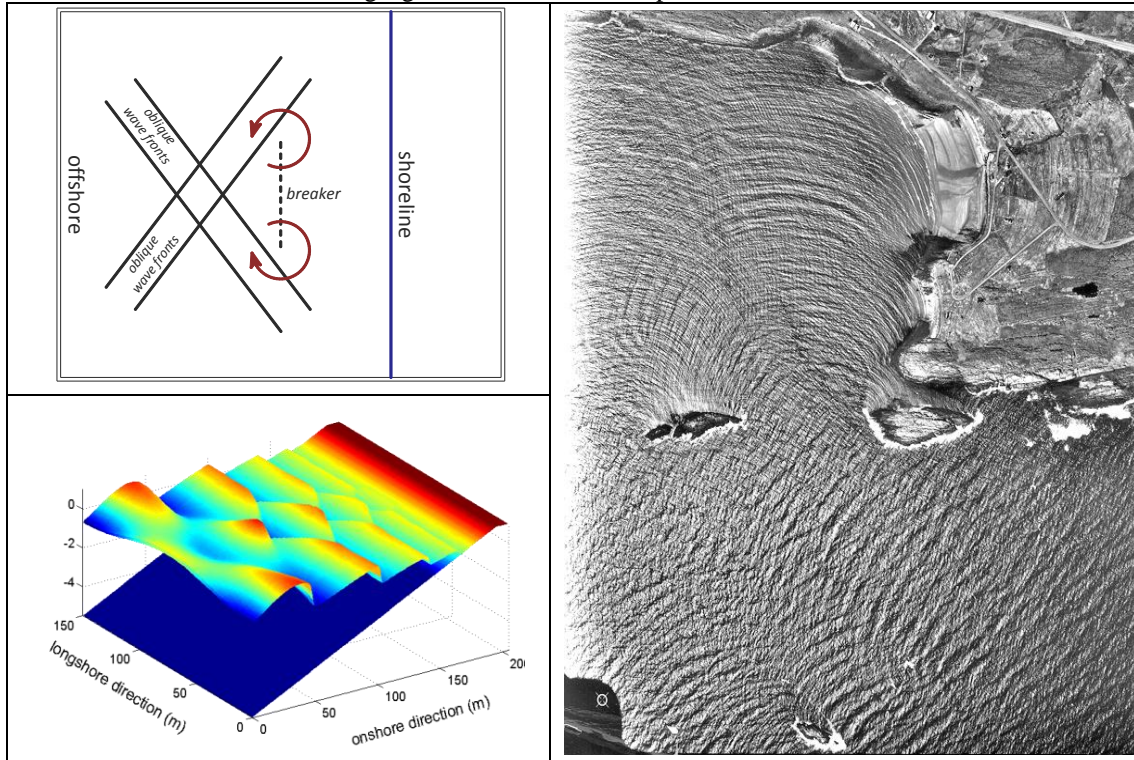


**Figure 1 – Sketch of the vorticity generation by wave-wave interaction (top left panel), short-crested system induced by the wave interaction (bottom left panel) and picture of the main processes related to the cross-sea condition (right panel).**

Many of the processes occurring in the nearshore region may induce cross-sea conditions and, thus, lead to breakers of finite longshore length. The most important are: i) the diffraction behind natural or artificial islands and behind breakwaters, ii) the refraction, due to bathymetry gradients, of consecutive waves, characterized by the same initial direction (e.g. in deep waters) and different celerity, iii) the reflection, due to natural or artificial walls, that generates a sort of “steady three-dimensional” wave pattern (right panel of Fig. 1).

The literature on the interaction of waves that leads to cross-sea conditions the nearshore is not abundant. Among the available papers we recall that describing the laboratory experiments by Fowler and Dalrymple (1990), who studied the influence of two incident wave trains, characterized by different frequency and inclination, on the evolution of rip currents. Other important studies about crossing waves have been undertaken by Craig and Nicholls (2002), who performed a perturbation analysis and some numerical computations of two- and three-dimensional periodic traveling water waves, and by Hammack et al. (2005), who compared experimental and numerical results of progressive obliquely-interacting wave trains in deep waters.

In the perspective of investigating the main features of the cross sea, especially in the presence of waves of different characteristics (height and period) and different angles to shore, a series of numerical simulations have been run by the NSW solver. The solver is based on a pseudoinviscid approach and makes use of a shock-capturing method.

Furthermore, starting from the ray (see, e.g. Mei 1983), that is used to investigate the refraction occurring over weakly varying bathymetries, we have built a new theory that enables to study the breaking location. The theory uses the shallow water approximation and some results are compared with the numerical results obtained from the NSW simulations.

Section 2 gives a description of the numerical model and introduces the numerical tests. In section 3 the cross-sea theory, derived from the original ray theory, is described. Section 4 shows the main results coming from both theory and simulations. Some conclusions close the paper.

### THE NUMERICAL FRAMEWORK

In the last decades several numerical models for the description of the nearshore flows have been arranged. Many of such models, starting from the three-dimensional Navier-Stokes equations, discretize the flow by means of a depth average, that represents a fairly good approximation in shallow waters: such models are called 2DH (two dimensional horizontally). The most common wave-resolving 2DH models are based on either Boussinesq-Type Equations (among others, Madsen et al. 1997) or Nonlinear Shallow Water Equations (e.g. Brocchini et al. 2001). Recently, hybrid models, that use both BTE and NSW, are representing the present fashion: the solver FUNWAVE-TVD by Shi et al. (2012) is an example.

Here below, a description of the NSW solver and an illustration of the numerical tests of cross sea, run with the code, are presented.

#### The numerical solver

The numerical solver here presented describes the hydrodynamics in the nearshore regions by using the NSW (details can be found in Brocchini et al. 2001). These are wave-resolving equations of conservation of mass and momentum, along  $x$  and  $y$ , and the involved variables are depth averaged:

$$d_t + (ud)_x + (vd)_y = 0, \quad (1)$$

$$u_t + uu_x + vv_y + gd_x = -gz_{b,x} + F_x - B_x, \quad (2)$$

$$v_t + uv_x + vv_y + gd_y = -gz_{b,y} + F_y - B_y, \quad (3)$$

where  $(x,y,z)$  are Cartesian orthogonal coordinates, being the still-water level  $z=0$ ;  $d(x,y,t) = \eta(x,y,t) + z_b(x,y,t)$  is the total water depth,  $\eta$  and  $z_b$  being, respectively, the free-surface level and the seabed with respect to the still-water level (see also Fig. 2);  $\mathbf{v}=(u,v)$  is the depth-averaged velocity vector,  $u(x,y,t)$  and  $v(x,y,t)$  being, respectively, the onshore and longshore components;  $F_x$  and  $F_y$  are the viscous terms;  $B_x = C_\tau |\mathbf{v}|u/d$  and  $B_y = C_\tau |\mathbf{v}|v/d$  are the friction terms, written in Chezy-type form;  $C_\tau$  is the dimensionless Chezy coefficient.

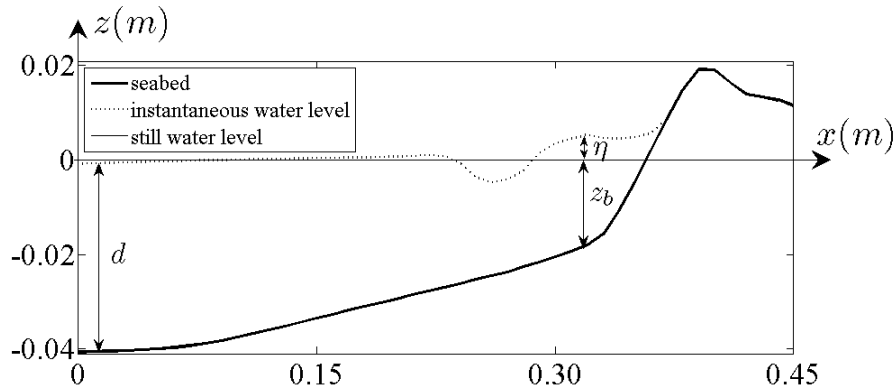


Figure 2 - Seabed profile (—) and free-surface elevation (···).

Hence, the solver takes into account both the seabed-friction contribution (through  $B_x$  and  $B_y$ ), fundamental in all the nearshore processes occurring in the surf zone (see Antuono et al. 2012) and the viscous contribution of the dissipative forces (through  $F_x$  and  $F_y$ ), i.e. i) turbulence, ii) secondary flows (compound-channel case), iii) wave breaking (nearshore case). Actually, for the present simulations, we use a pseudoinviscid approach ( $F_x=F_y=0$ ) and the breaking is described as a shock, i.e. a simple water level discontinuity (see Whitham 1974).

The NSW solver discretizes equations (1)-(3) by using a conservative finite-volume method and evaluates the intercell fluxes by means of Weight Averaged Flux (WAF) method. A TVD scheme is also applied to avoid spurious oscillations due to discontinuous solutions.

### The numerical simulations

Several configurations of cross sea have been tested, each lasting 250s. The bathymetry is characterized by a flat sloping beach (slope  $i=1/30$ ) inside a domain where  $x=(0-205)m$  and  $y=(0-150)m$ . Such a domain is identical to that used for the numerical simulations of Brocchini et al. (2004), where the flat beach was interrupted by a single submerged breakwater. The spatial discretization is  $\Delta x=1m$  and  $\Delta y=2m$  along  $x$  and  $y$ , respectively.

All the tested waves are regular and the input characteristics (height  $H_0$  and period  $T_0$ ) are given at the offshore boundary ( $x=0$ ) in the form of a time series of both water elevation and velocity. The number of wave trains traveling from the offshore to the inshore ( $n$ ) and the inclination of each of them ( $\theta_i$ , with  $i=1:n$ ) are also given as boundary conditions. Table 1 shows all the characteristics of the tests where the number of wave trains is  $n=2$  (A-type tests) and such trains are symmetrical with respect to the center of the domain (at  $y=75m$ ). The same waves, with an additional train characterized by  $\theta_3=0^\circ$ , have been used to run 12 tests more (B-type tests): e.g. the test characterized by  $H_0=0.5m$ ,  $T_0=5s$ ,  $\theta_1=30^\circ$ ,  $\theta_2=-30^\circ$  and  $\theta_3=0^\circ$ , is the test 1.B.

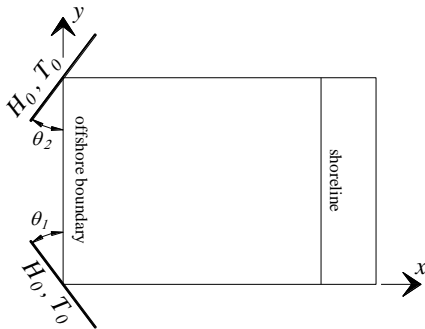


Figure 3 – Main characteristics of the numerical domain.

Test name	$H_0$ (m)	$T_0$ (s)	$\theta_1$ ( $^\circ$ )	$\theta_2$ ( $^\circ$ )
1.A	0.5	5	30	-30
2.A	0.5	5	45	-45
3.A	0.5	5	60	-60
4.A	1.0	5	30	-30
5.A	1.0	5	45	-45
6.A	1.0	5	60	-60
7.A	0.5	10	30	-30
8.A	0.5	10	45	-45
9.A	0.5	10	60	-60
10.A	1.0	10	30	-30
11.A	1.0	10	45	-45
12.A	1.0	10	60	-60

### THE APPROXIMATED CROSS-SEA THEORY

In order to understand how waves modify when they travel over a sloping beach, an important theory was built, based on Snell's law of refraction. Similarly to what happens to the light when passing through the interface between two media characterized by different index of refraction, the direction of a wave changes when it is traveling over a sloping beach: the water depth plays the same role of the index of refraction. Some decades ago, based on the refraction law, Mei (1983) presented the theory of wave rays that, while approaching the shore, tend to become orthogonal to the shore. The water volume in between two rays is called "ray channel" and it enlarges going from the offshore to the inshore, i.e. the more the water depth reduces, the more the rays widen.

We here apply the ray theory, under the assumption of steady-state waves, to the cross-sea condition. Hence, we assume a scheme that is slightly different from that of Mei (1983) because takes two wave rays that, approaching the shore over a sloping beach, converge. This represents the main difference between the ray theory and the new "cross-sea theory", both following the main assumption of energy conservation. The sketch of such a new interpretation of the ray channel is shown in the left panel of Fig. 4.

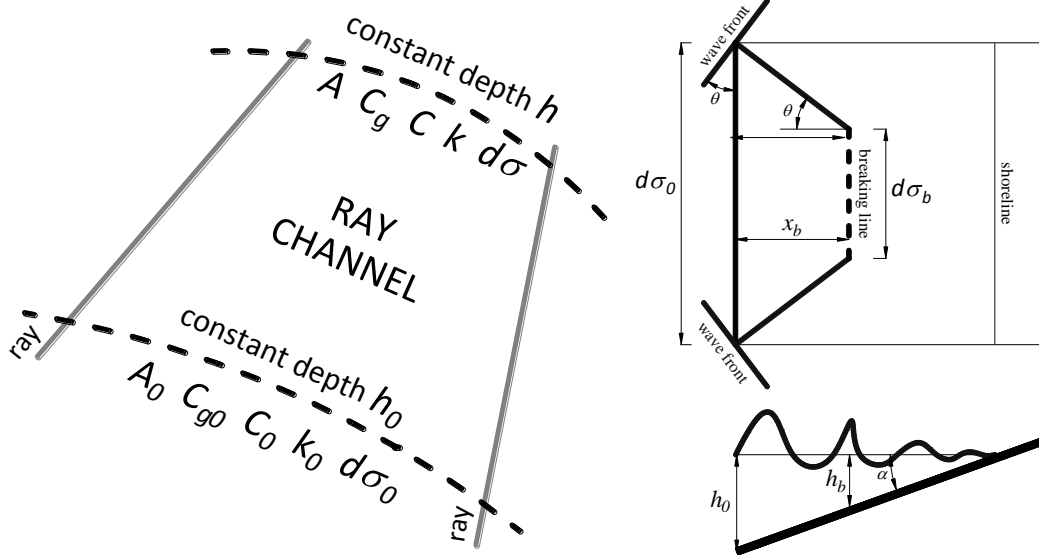


Figure 4 – Cross-sea theory applied to a generic bathymetry (left) and to a beach of fixed slope: planar (top right) and cross-shore (bottom right) view.

The left panel of Fig. 4 illustrates how the new theory works in the presence of two rays, associated to two wave trains approaching the shore with different angles: in correspondence to a certain depth ( $h_0$ ) both rays are characterized by an amplitude ( $A_0$ ), a celerity ( $C_0$ ), a group velocity ( $C_{g0}$ ) and a wave number ( $k_0$ ). At that position the ray-channel width is  $d\sigma_0$ . While approaching the shore, the rays come closer and, at a depth  $h$ , all the characteristics change ( $A, C, C_g, k, d\sigma$ ). Following Mei (1983):

$$\frac{A}{A_0} = \sqrt{\frac{C_{g0}}{C_g} \frac{d\sigma_0}{d\sigma}} = \sqrt{\frac{\frac{C_0}{2} \left(1 + \frac{2k_0 h_0}{\sinh(2k_0 h_0)}\right)}{\frac{C}{2} \left(1 + \frac{2kh}{\sinh(2kh)}\right)} \frac{d\sigma_0}{d\sigma}} \quad (4)$$

If we consider to work in shallow waters (i.e.  $k_0 h_0$  and  $kh \ll 1$ , hence  $\sinh(2k_0 h_0) \cong 2k_0 h_0$  and  $\sinh(2kh) \cong 2kh$ ), we can simplify Eq. 4:

$$\frac{A}{A_0} \cong \sqrt{\frac{\sqrt{gh_0}}{\sqrt{gh}} \frac{d\sigma_0}{d\sigma}} = \left(\frac{h_0}{h}\right)^{\frac{1}{4}} \left(\frac{d\sigma_0}{d\sigma}\right)^{\frac{1}{2}}, \quad (5)$$

from which it is clear that the wave amplitude increases moving shoreward ( $A/A_0 > 1$ ), because  $h_0 > h$  (depth variation) and  $d\sigma_0 > d\sigma$  (mutual interaction of rays).

Given that waves may be taken as linear only if they are not breaking, we decide to use the breaking line as the limit of our theory. Hence, as illustrated in the right panel of Fig. 4, we assume that the cross-sea theory holds from the offshore (outer boundary) to the breaking line (inner boundary), and it is defined in a convergent channel defined between two rays representing the obliquely incident wave trains (side boundaries). As a consequence, we can substitute the variables referring to a generic depth  $h$ , appearing in Eq. 5, with those referring to the depth of the breaking line  $h_b$ . We obtain:

$$\frac{A_b}{A_0} = \left(\frac{h_0}{h_b}\right)^{\frac{1}{4}} \left(\frac{d\sigma_0}{d\sigma_b}\right)^{\frac{1}{2}}, \quad (6)$$

where the wave amplitudes can be taken as  $A_b = H_b/2$  and  $A_0 = H_0/2$ , where  $H_b$  and  $H_0$  are, respectively, the wave heights at the breaking location and at the offshore boundary.

From the right sketches of Fig. 4 it is possible to extract further geometrical rules to evaluate some of the unknowns of Eq. 6. If the two wave trains are characterized by the same (in modulus) inclination  $\theta$ , from the top right sketch of Fig. 4 we have:

$$\frac{d\sigma_0 - d\sigma_b}{2} = x_b \tan \theta \quad (7)$$

and from the bottom right sketch we can derive:

$$h_b = h_0 - x_b \tan \alpha , \quad (8)$$

where  $\alpha$  is the beach slope.

For the evaluation of the breaking wave height we use the simple criterion that directly connect it to the water depth (Dean 1968):

$$H_b = \gamma h_b , \quad (9)$$

where  $\gamma$  is a constant ranging between 0.73 and 0.87.

Combination of Eqs. 6, 7, 8 and 9 leads to the following equation:

$$(h_0 - x_b \tan \alpha)^5 (d\sigma_0 - 2x_b \tan \theta)^2 = \frac{H_0^4 h_0 d\sigma_0^2}{\gamma^4} , \quad (10)$$

for which no explicit solutions exist.

#### Application of the cross-sea theory

To compare theoretical and numerical results, we decide to solve Eq. 10 using the input values of the numerical simulations, some of them illustrated in Table 1. The only unknown in Eq. 10 is the breaking location  $x_b$ , hence the used boundary parameters are:  $h_0=5.5\text{m}$ ;  $d\sigma_0=150\text{m}$ ;  $i=\tan\alpha=1/30$ ;  $H_0=0.5\text{m}, 1.0\text{m}$ ;  $\theta=|\theta_1|=|\theta_2|=30^\circ, 45^\circ, 60^\circ$ .

Since the wave period is not taken into account in Eq. 10 because of the shallow water approximation (see Eqs. 4 and 5), such a theory give the same results if the wave trains are characterized by either  $T_0=5\text{s}$  or  $T_0=10\text{s}$ . Further, such a theory is only valid for two incident wave trains converging and focusing in a unique breaking line, this enabling us to disregard the numerical tests where  $n=3$ .

## RESULTS

In this section results of both numerical simulations and cross-sea theory are presented. In the beginning, some clarifications about the way we choose the breaking point in the numerical domain are given. Then, comparisons between results coming from theory and from numerical simulations are illustrated. Some results about vorticity and vortex trajectories are shown in the last subsection.

#### Identification of the breaking position in the numerical tests

We extrapolate the breaking position  $x_b$ , with respect to the offshore boundary, from the numerical results of the water level  $\eta$  at the different time steps and in correspondence of the central cross section (i.e.  $y=75\text{m}$ ). Fig. 5 illustrates all the water level outputs obtained from  $t=200\text{s}$  and  $t=250\text{s}$ , with step  $\Delta t=2\text{s}$ . Among all the outputs, the maximum water elevation (highlighted by a black circle in Fig. 5) represents the breaking point. Hence, at that location we have both  $h_b$  and  $x_b$ .

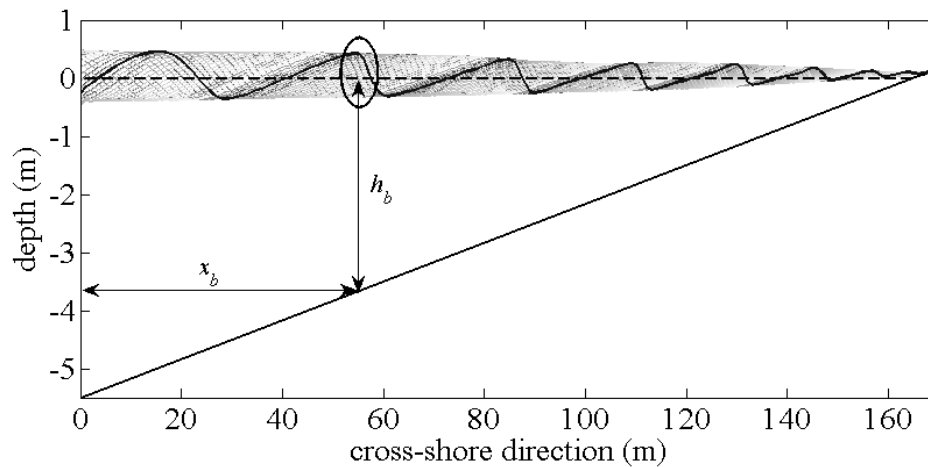


Figure 5 – Individuation of the breaking location from the numerical tests.

### Comparison between cross-sea theory and NSW simulations

The comparison between analytical solutions of the cross-sea theory and results of the numerical tests refers to the localization of the breaking waves  $x_b$ . According to the numerical tests carried out using the NSW and described in Table 1, the solution of Eq. 10 have been found for the same cases and using a breaking parameter  $\gamma=0.78$ . Input data and results of Eq. 10 are summarized in **Errore. L'origine riferimento non è stata trovata.**

$d\sigma_0$ (m)	150	150	150	150	150	150
$h_0$ (m)	5.5	5.5	5.5	5.5	5.5	5.5
$i$	1/30	1/30	1/30	1/30	1/30	1/30
$\gamma$	0.78	0.78	0.78	0.78	0.78	0.78
$H_0$ (m)	0.5	0.5	0.5	1	1	1
$\theta$ (°)	30	45	60	30	45	60
$x_b$ (m)	104	70	42	82	60	38

Since the cross-sea theory is only valid in the shallow water field, i.e.  $kh \ll 1$ , as imposed to have Eq. 5, there is no influence of wave period  $T_0$  on the solution. Hence, each analytical result is compared with the results obtained from two numerical tests, because two different wave periods ( $T_0=5s$  and  $10s$ ) have been used for each combination of wave height ( $H_0$ ) and wave-train inclination ( $\theta$ ). The comparison is illustrated in Fig. 6.

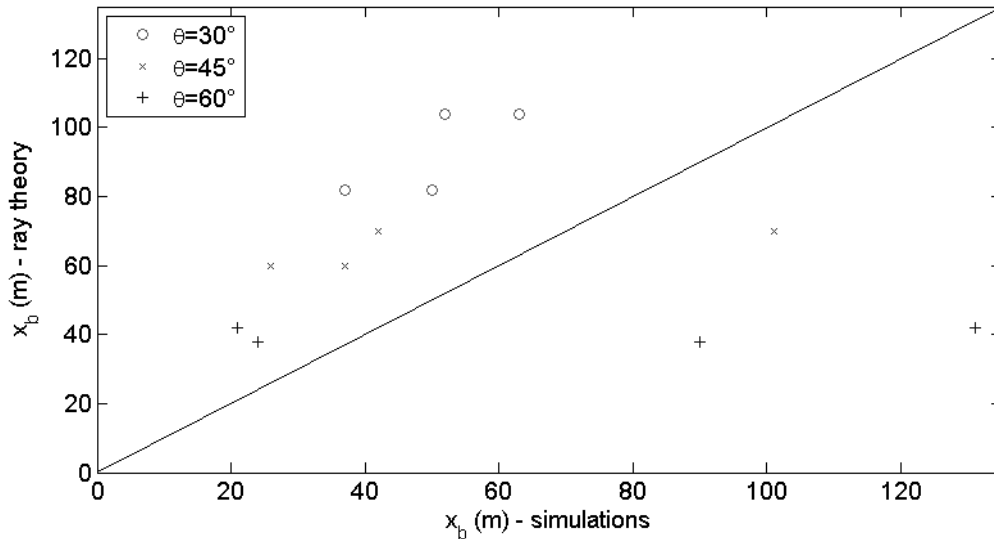


Figure 6 - Comparison between results of numerical simulations and theoretical solutions for different wave angles:  $\theta=30^\circ$  (o),  $45^\circ$  (x) and  $60^\circ$  (+).

Fig. 6 shows quite different results between numerical and theoretical values of the breaking position, probably due to either the approximation of the cross-sea theory, i.e. a linear theory is compared with a numerical model built on nonlinear equations, or the breaking phenomenon in the NSW framework, that is predicted early because of the absence of dispersive terms.

#### Vorticity patterns and vortex trajectories

In order to investigate similarities with the nearshore hydrodynamics generating when submerged obstacles are present in the domain, the vorticity field has been analyzed. In fact, similarly to a configuration with a planar beach protected by submerged breakwaters (see Brocchini et al. 2004, hereinafter BR04, and Kennedy et al. 2006, hereinafter KE06), breakers of finite length generate as a consequence of the short-crested system induced by the cross sea.

Such a mechanism, as well as what happens in between two contiguous breakwaters (see, for details, KE06), is mainly characterized by the generation of counter-rotating vortices at the edges of the breaker, corresponding to the heads of each structure in the case described by KE06.

In the presence of submerged breakwaters, offshore-directed currents, also known as rip currents, generate in the gap between such barriers, because of the different water level between the protected part of the beach and the offshore. Such currents are responsible of the vortices motion, that detach from the breakwater edges and are transported seawards, also enforced by the mutual advection due to their opposite sign, as described in BR04.

In the cross-sea condition case the generation of finite-length breakers leads to a pair of counter-rotating vortices, as sketched in the left panel of Fig. 1. The mechanism is similar to that described by KE06 in the presence of gaps width equal to breakwaters length (wider rip-current case). The coupling between vortices generated by close breakers enables the mutual-advection mechanism and makes all the vortices of the domain move toward the offshore.

As an example, we here show (Fig. 7) some instants that are significant for the vorticity patterns generating in the numerical domain during test 2.B, characterized by  $H_0=0.5\text{m}$ ,  $T_0=5\text{s}$ ,  $\theta_1=45^\circ$ ,  $\theta_2=-45^\circ$  and  $\theta_3=0^\circ$ . In particular, such a simulation has been run for more than 250s, used for all the tests, to observe the vorticity evolution and the vortex paths up to the offshore end of the domain. In this specific case, the generation of counter-rotating vortices is evident in the central part of the domain, i.e. at  $y=(60-80)\text{m}$ , during the first 150s (panels a, b, c). In the next instants (between 180s and 240s, panels d, e, f), the central vortices enlarge because attracted by other large eddies generated laterally, i.e. at about  $y=30\text{m}$  and  $y=120\text{m}$ , these enabling the mutual-advection mechanism to occur. Such a mechanism pushes the new pairs of vortices, one in the top part of each panel ( $y>80\text{m}$ ), one in the bottom part ( $y<70\text{m}$ ), to the offshore boundary and force them to also move laterally, i.e. toward the closest lateral boundary. This is clear especially for  $t=(240-300)\text{s}$  (see panels f, g, h).

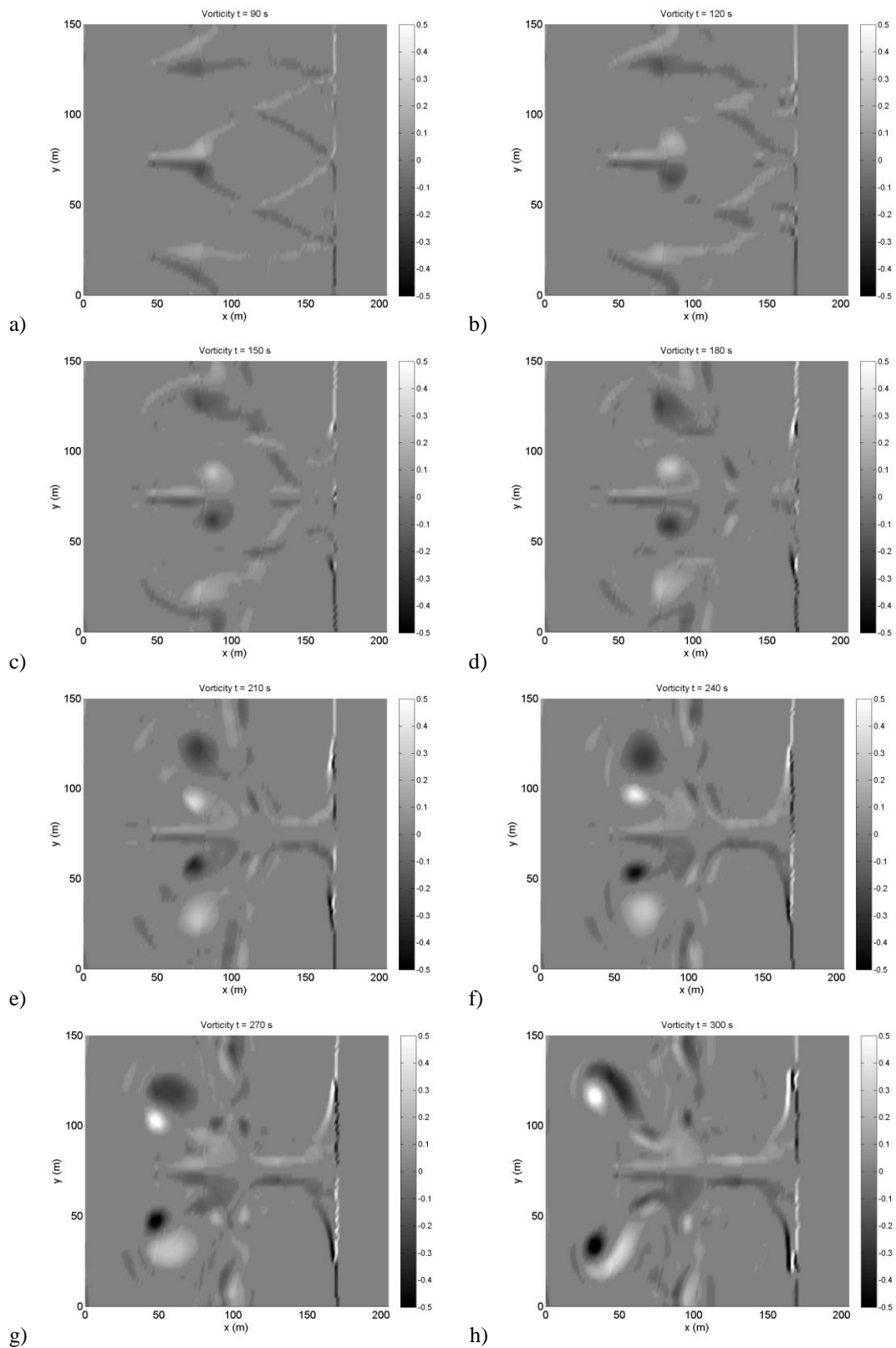


**Figure 7 - Vorticity-patterns evolution for the case 2.B at different times: a)  $t=90s$ , b)  $t=120s$ , c)  $t=150s$ , d)  $t=180s$ , e)  $t=210s$ , f)  $t=240s$ , g)  $t=270s$ , h)  $t=300s$ .**

The obtained pattern is, hence, similar to that obtained in the case of a rip current in the presence of a submerged isolated breakwater (see the experimental results of KE06) and the main direction of both

pairs is inclined of about  $25^\circ$  with respect to the  $x$  axis (see left panel of Fig. 8, where trajectories of the two central vortices are plotted).

Results presented in Fig. 7 are quite similar, but not identical, to those found when only two inclined waves (A-type tests) are forced in the numerical domain. In such cases the trajectories of both pairs of vortices seem to be almost orthogonal to the offshore boundary, the case with  $|\theta_1| = |\theta_2| = 45^\circ$  being characterized by the most rapid vortices. In fact, for what concerns tests 1.A and 3.A, the former is characterized by both pairs of vortices almost stuck around  $x=100\text{m}$ , the latter by vortices fixed at around  $x=125\text{m}$ . For the case 2.A, characterized by the same inputs of the previously mentioned tests except for the wave-train inclination, two rip currents are clearly visible, as shown in the right panel of Fig. 8. As already mentioned, such currents, that refer to the central counter-rotating vortices, seem to be almost orthogonal to the  $y$  axis.

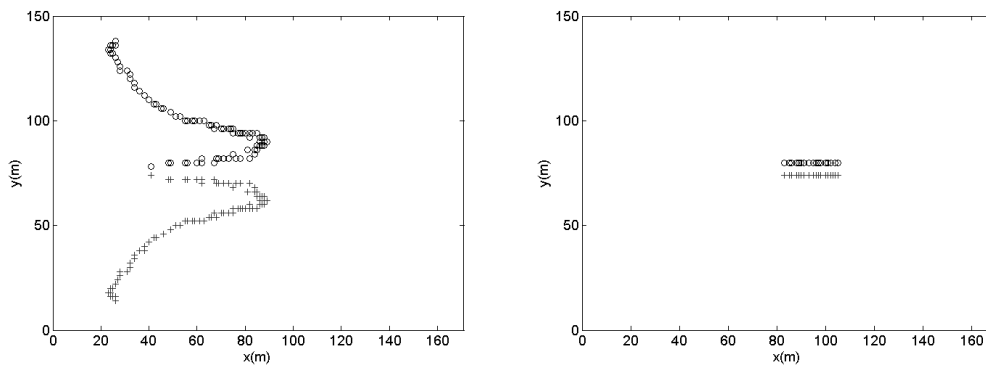


**Figure 8 –Trajectories of the central counter-rotating vortices for the long-duration test 2.B (left) and for test 2.A (right): positive counter-clockwise (o) and negative clockwise (+) vortices.**

## CONCLUSIONS

In the present work, the scope of investigating the cross-sea condition case has been undertaken by both running some numerical simulations, using a NSW solver, and developing a new theory, starting from the well-known ray theory (Mei 1983). Different cross-sea conditions have been tested using the numerical solver, changing both the characteristics of the input waves (height and period), the inclination of the wave trains and the number of the incoming wave trains. For each simulation the breaking point has been found from the central cross-section of the domain.

Since the new theory has been approximated accounting for the shallow water condition, some comparisons have been made on the basis of the distance of the breaking point from the offshore boundary, but non perfect match has been found between numerical and analytical results.

Concerning the vorticity generation in the numerical domain, patterns similar to that occurring in the presence of submerged obstacles, such as breakwaters, have been found, with vortices propagating towards the offshore with different speed and angles, depending on both inclination and number of the wave trains.

## REFERENCES

- Antuono, M., L. Soldini, and M. Brocchini. 2012. On the role of the Chezy frictional term near the shoreline, *Theoretical and Computational Fluid Dynamics*, 26, 105-116.
- Brocchini, M., R. Bernetti, A. Mancinelli, and G. Albertini. 2001. An efficient solver for nearshore flows based on the WAF method, *Coastal Engineering*, 43, 105-129.
- Brocchini, M., A.B. Kennedy, L. Soldini, A. Mancinelli. 2004. Topographically controlled, breaking-wave-induced macrovortices. Part 1. Widely separated breakwaters, *Journal of Fluid Mechanics*, 507, 289-307.
- Craig, W., and D.P. Nicholls. 2002. Traveling gravity water waves in two and three dimensions, *European Journal of Mechanics B/Fluids*, 21, 615-641.
- Dean, R.G. 1968. Breaking wave criteria; a study employing a numerical wave theory, *Proceedings of the 11<sup>th</sup> International Conference on Coastal Engineering*, 108-123.
- Fowler, R.E., and R.A. Dalrymple. 1990. Wave group forced nearshore circulation, *Proceedings of 22<sup>nd</sup> International Conference on Coastal Engineering*, ASCE, 729-742.

- Hammack, J., D.M. Henderson, and H. Segur. 2005. Progressive waves with persistent two-dimensional surface patterns in deep water, *Journal of Fluid Mechanics*, 532, 1-52.
- Kennedy, A.B., M. Brocchini, L. Soldini, E. Gutierrez. 2004. Topographically controlled, breaking-wave-induced macrovortices. Part 2. Changing geometries, *Journal of Fluid Mechanics*, 559, 57-80.
- Madsen, P.A., O.R. Sørensen, and H.A. Schäffer. 1997. Surf zone dynamics simulated by a Boussinesq type model. Part I. Model description and cross-shore motion of regular waves, *Coastal Engineering*, 32, 255-287.
- Mei, C.C. 1983. *The applied dynamics of ocean surface waves*, Wiley-Interscience, 740 pp.
- Shi, F., J.T. Kirby, J.C. Harris, J.D. Geiman, and S.T. Grilli. 2012. A high-order adaptive time-stepping TVD solver for Boussinesq modelling of breaking waves and coastal inundation, *Ocean Modelling*, 43-44, 36-51
- Silvester, R. 1974. *Coastal Engineering II*, Elsevier, Amsterdam, 338 pp.
- Whitham, G.B. 1974. *Linear and nonlinear waves*, John Wiley & Sons, New York.